Dynamic Light-Scattering Studies of Polymer Diffusion in Porous Materials: Linear Polystyrene in Porous Glass

Matthew T. Bishop,[†,‡] Kenneth H. Langley,[*,§] and Frank E. Karasz[†]

Polymer Science and Engineering Department and Department of Physics and Astronomy, University of Massachusetts, Amherst, Massachusetts 01003. *Received June 29, 1988*

ABSTRACT: The molecular weight dependence of the translational diffusion coefficient of a flexible polymer in a highly interconnected porous glass material has been studied by using dynamic light scattering. Porous silicas, each with different pore radius R_P and porosity Φ, were saturated at equilibrium with dilute solutions of linear polystyrene in a thermodynamically good solvent and examined in a light-scattering spectrometer. Each measurement of diffusion was made entirely inside a single fragment of saturated porous material, thus eliminating effects due to movement of polymer from unbounded solution into the porous material. Diffusion behavior was investigated as a function of the dimensionless variables $\lambda_H \equiv R_H/R_P$ (the size of the polymer relative to the pores) and qR_P (essentially the ratio of pore size to the length over which diffusion is probed), where R_H is the polymer hydrodynamic radius and q the scattering wave vector. Macroscopic diffusion coefficients, D_∞, phenomenological coefficients for diffusion over large distances in the porous glass, were obtained from data at low qR_P. The reduction in D_∞ relative to D_0, where D_0 is the diffusivity in unbounded solution, can be satisfactorily interpreted in terms of (1) hydrodynamic interactions of the polymer with the pore walls, which lead to a reduced intrapore diffusivity, D_P, relative to D_0, and (2) the tortuosity of the pore space. At small λ_H ($\lambda_H \leq 0.23$), the reduction in D_P/D_0 with increase in λ_H is in good quantitative agreement with models for diffusion of hard spheres in isolated cylindrical pores, even though the pore space of these glasses is highly interconnected. The appropriate effective hard-sphere radius is identified as the hydrodynamic radius R_H. At higher λ_H ($\lambda_H > 0.18$), the dependence of D_P/D_0 on λ_H is consistent with a transition from non-free-draining to free-draining behavior as is predicted by scaling theories, although the limited range of λ_H ($\lambda_H \leq 0.47$) prevents drawing any strong conclusions. For these data, the tortuosities (obtained as the inverse of D_∞/D_0 in the limit $\lambda_H = 0$) are related to the pore space geometry and are independent of λ_H.

Introduction

The diffusivity of a polymer molecule in a pore of comparable size differs from that in unbounded solution. First, the hydrodynamic interaction between polymer and pore walls leads to increased drag and substantially "hindered" diffusion.[1-5] Second, for flexible polymers, overall hydrodynamics are complicated by changes in intrachain hydrodynamics[6-8] as caused by changes of polymer configuration inside pores.[9]

Recent studies have focused mainly on the diffusive transport of various species—small molecules,[10] spherical colloids,[11,12] flexible polymers,[13-18] and polymers with fixed configuration[15,16]—across track-etched membranes, which are geometrically simple and which correspond closely to the cylindrical pore model that has been extensively used in theoretical work. For flexible polymers, the results of membrane transport experiments have been found to be generally consistent with theories for the diffusion of hard spheres in cylindrical pores[1-5] (which are based on the results of low Reynolds number hydrodynamics plus simple steric partitioning) and also with scaling theories[6-9] (which take into account the effect of chain flexibility on both the partitioning coefficient[9] and intrachain hydrodynamics[6-8]). Certain results are explained only by scaling theories.[14,18] The appropriate flexible polymer radius to use as an effective hard sphere radius (R_S) remains an outstanding question. Results for polystyrene[13] and star polyisoprene[17] have indicated that R_S/R_H is significantly greater than 1, whereas those for dextran[16] and linear polyisoprene[17] have implied that R_S/R_H is significantly less than 1.

For diffusion in porous materials more geometrically complex than track-etched membranes, consideration of these hydrodynamic effects alone is insufficient to relate macroscopic diffusion behavior to microscopic parameters characterizing the diffusant and the porous material. Such systems, although of greater technological importance, have been studied much less. The diffusion of polystyrene in porous glasses, which have highly interconnected and somewhat random pore spaces, has previously been examined by transient diffusion[19,20] and by diffusional peak broadening in size exclusion chromatography.[21,22] The results of these previous experiments,[19-22] which are in conflict with theories for hindered diffusion and with the results of membrane transport experiments, provided much of the motivation for the present work.

We have recently applied the technique of dynamic light scattering to this same system (i.e., polystyrene in porous glass)[23] and here present studies of the spatial and molecular weight dependence of diffusion behavior in three different glasses. Contrary to previous results,[19-22] we find that the diffusion behavior of flexible polymers in these porous glasses is in no way unusual. Our results, which are consistent with the results of previous membrane transport experiments, can be understood by combining phenomenological theories for the diffusion of point particles in random porous materials[24-26] with theories for diffusion of hard spheres[1-5] and flexible polymers[6-8] in pores of simple geometry.

Dynamic light scattering[27,28] has previously been applied to related problems: hindered diffusion of spherical colloids between parallel plates;[29,30] fundamental aspects of Brownian motion near a wall;[31] probe polymer diffusion in polymer matrices (e.g., see references cited in ref 32). It offers several significant advantages compared to phenomenological experimental approaches such as membrane transport and transient diffusion. Measurements are made at equilibrium within the porous material, not in a surrounding reservoir, and directly reflect the Brownian motion of the diffusing polymer within the pores. Very importantly, in contrast to most other approaches, these light-scattering experiments are also such that the equilibrium partitioning coefficient[9,33-35] of polymer between unbounded solution and pore space does not have to be known. This allows for a more direct examination of the polymer dynamics per se, without confounding by partitioning. The primary limitation of the technique lies in the requirements that the porous material must be opti-

[†] Polymer Science and Engineering Department.
[‡] Present address: Dow Chemical Co., Midland, MI 48640.
[§] Department of Physics and Astronomy.

0024-9297/89/2222-1220$01.50/0

Table I
Polystyrene Sample Characteristics[a]

code	supplier (lot)	$10^{-3}M_p$	$10^{-3}M_D$	10^7D_0, cm^2/s
21k	PC (41220)	17.5	21.3	14.4
33k	PC (80317)	35	33.1	11.2
53k	PC (60917)	50	53.2	8.55
102k	PC (70111)	100	102	5.92
181k	PC (30126)	170	181	4.26
401k	PC (507)	300	401	2.71
406k	PC (3b)	390	406	2.69
583k	PC (30121)	575	583	2.19
1050k	PL	1030	1050	1.56
1380k	PL	1400	1380	1.34
2120k	PL	2050	2120	1.05

[a] Suppliers: PC = Pressure Chemical, PL = Polymer Laboratories. M_p = peak molecular weight from size exclusion chromatography. M_D = molecular weight back-calculated from power law relationship between D_0 and M_p. D_0 = diffusion coefficient in 2-fluorotoluene, at $c \approx c^*/8$, corrected to T = 42.6 °C and η_0 = 0.005 23 P.

cally transparent and have a refractive index that can be matched by a suitable solvent.

Experimental Section

Basic Description of the Experiments. Each sample for light scattering consisted of a single fragment of porous glass immersed in a dilute solution of polystyrene. The solvent was 2-fluorotoluene (Aldrich Chemical, 99+% pure, used as received). This thermodynamically good solvent for polystyrene was used to nearly, but not exactly, match the refractive index of the porous glass, with the scattering from the nearly index-matched glass providing a local oscillator for heterodyne[27,28] dynamic light-scattering measurements of diffusion within the porous glass, under conditions of macroscopic equilibrium.

Preparation of Light-Scattering Samples. Characteristics of the linear anionic polystyrenes are given in Table I. These samples had relatively narrow molecular weight distributions ($M_w/M_n \leq 1.06$). Mutual diffusion coefficients in bulk solution D_0, measured at finite concentrations ($c \approx c^*/8$, with c^* the overlap concentration[8]), were used to obtain the power laws

$$D_0 \text{ (42.6 °C, 0.005 23 P)} = (4.18 \times 10^{-4})M_p^{-0.569} \text{ cm}^2/\text{s} \quad (1a)$$

$$R_H \text{ (42.6 °C, 0.005 23 P)} = 0.106M_D^{0.569} \text{ Å} \quad (1b)$$

The value of the scaling exponent (0.569 ± 0.007) confirms that 2-fluorotoluene is a thermodynamically good solvent. Equation 1a was used to back-calculate the self-consistent molecular weights M_D from D_0. The Stokes–Einstein relation was used to operationally define an apparent hydrodynamic radius, $R_H \equiv kT/6\pi\eta_0 D_0$.

Dilute solutions of polystyrene in 2-fluorotoluene were prepared by allowing the polymer to slowly dissolve (e.g., 2 weeks for the highest molecular weights) with occasional gentle agitation. The concentration of each solution was scaled relative to c^* ($c \approx c^*/8$), where c^* was estimated from M_D as $c^* = [\eta]^{-1}$.

Each solution was filtered into two dust-free scattering cells (10 × 75 mm test tubes), one of which contained a firmly mounted and centered piece of silanized porous glass, the other a control. The cutoff size of the Fluoropore membrane filters (Millipore Corp.) was chosen to avoid removal of polymer from solution. Although small amounts of dust were introduced with the glass fragment assemblies, no evidence was seen for significant penetration into the relatively small pores (in all cases less than 0.4-μm diameter, similarly sized as the membrane filters) of the glasses. Sufficient time was allowed for polymer solutions to totally penetrate glass fragments before making measurements.

Porous Glass Samples. Three samples were used (Table II). Two were obtained commercially (Electro-Nucleonics): CPG1400 (lot 09D02, code R893) and CPG3000 (lot 11D10, code R1866). The third (code R703) was provided by Dr. Wolfgang Haller of the National Bureau of Standards. All three of these samples were "controlled pore" glasses (CPGs), which are made by a several step process[36] that ultimately produces a porous silica skeleton, typically 96% SiO_2. The commercial glasses were supplied with nominal pore radii R_P and specific pore volumes v_P (from mercury porosimetry) and specific pore surface areas a_P (from BET nitrogen adsorption measurements); these were also independently characterized by mercury porosimetry (Quantachrome Corp.). Insufficient quantity of glass R703 was available for any such testing.

Table II
Porous Glass Characteristics[a]

	glass code		
	R703	R893	R1866
v_P, cm^3/g	0.38	1.17	0.75
Φ	0.46	0.72	0.62
R_P, Å	703	893	1866
a_P, m^2/g		17.6	6.36
$2\sigma^{-1}$, Å		1318	2170
$2\sigma^{-1}/R_P$		1.45	1.15
X	0.58	0.78	0.78
T	1.73	1.28	1.28
F	3.77	1.78	2.07

[a] Quantities in this table are specific pore volume v_P; porosity Φ; median (50% intrusion) pore radius R_P from mercury porosimetry, using γ_{Hg} = 480 dyn/cm for the mercury surface tension and θ_A = 140° for the advancing contact angle; specific pore surface area a_P; hydraulic radius σ^{-1}; intrinsic conductivity X; tortuosity T; and formation factor F.

Scanning electron micrographs (Figure 1) illustrate the structure of these CPGs. The highly interconnected pore space is bicontinuous with the silica skeleton. Also, all pores are connected to the outside surface. Viewed with magnifications scaled as $1/R_P$ (Figures 1a–c), the two commercial glasses (R893 and R1866) look similar to each other but different from the Haller glass (R703).

Porosities Φ were obtained from specific pore volumes v_P as $\Phi = v_P/\{v_P + (1/\rho)\}$, with ρ = 2.2 g/cm^3 the density of silica. Values of v_P were obtained from the uptake of fluid per gram of glass, either from mercury porosimetry (R893 and R1866) or from solvent sorption (R703).

Mercury porosimetry results[41] for glasses R893 and R1866 indicate that these CPGs have remarkably narrower pore size distributions than do most porous materials, with about 90% of the volume intruded within ±7% of the median R_P values. However, although mercury porosimetry is experimentally straightforward, the extraction of pore size information from such data is less so.[37,38] The following discussion thus anticipates questions that subsequently arise in making a quantitative comparison between our hindered diffusion data and theory.

Calculation of the distribution of incremental pore volume associated with a given radius of equivalent cylindrical pores was based on the Laplace equation. Assuming cylindrical pore geometry, pressure p was converted to pore radius r_P as

$$r_P = 2\gamma_{Hg} \cos \theta_A/p \quad (2)$$

where γ_{Hg} is the surface tension of mercury and θ_A is the advancing contact angle.[37] Although the pores are obviously not cylindrical (Figure 1), leading to ambiguity in the relation of R_P values (Table II) to actual pore geometry, the values should be correct in at least a relative sense, given the similar pore space geometries of these three glasses.

That these R_P values should be reasonably accurate in even an absolute sense is supported by a previous study on CPGs from Electro-Nucleonics, which claimed to show excellent agreement between R_P measurements by mercury porosimetry and electron microscopy.[39] The accuracy of R_P values also rests on proper choice (Table II) of mercury surface tension γ_{Hg} and especially the advancing contact angle θ_A. (There is controversy[38] as to the correct value of θ_A, with suggested values ranging from 130° to 180°.)

When there are larger pores accessible only through smaller pores ("ink bottles"), mercury porosimetry will underestimate, potentially severely, both the average pore size and the breadth of the size distribution.[37,38] The ratio $2\sigma^{-1}/R_P$, with $\sigma^{-1} = v_P/a_P$, provides an idea of the underestimation of pore size, since the hydraulic radius σ^{-1} is equal (or very nearly so) to half the porosimetry "radius" r_P for a single pore of *any* regular geometry. Consider a network with pores of two different radii ($R_2 = 2R_1$), with equal volume associated with each radius, but with all volume

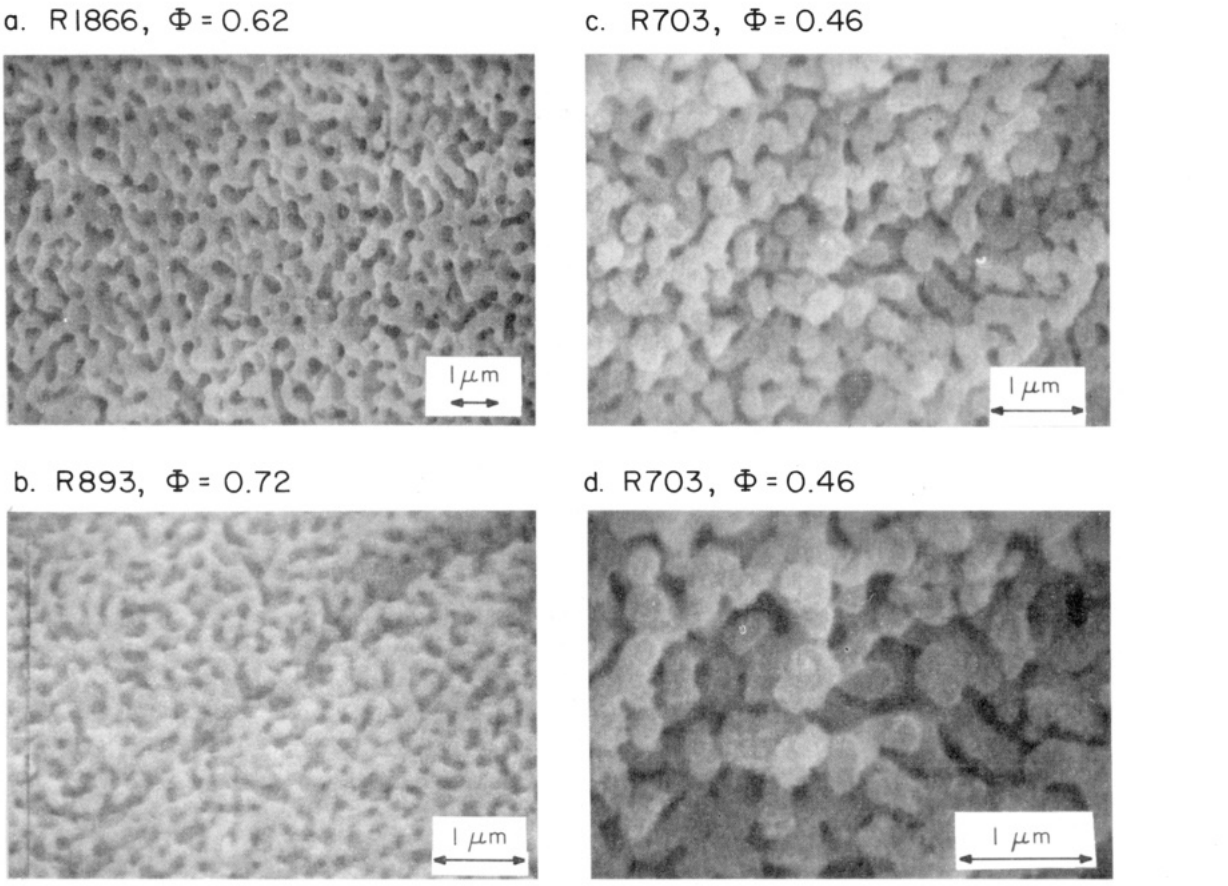

Figure 1. Scanning electron micrographs of porous glasses, coated with 100–200 Å of gold. Magnifications in a–c are roughly proportional to $1/R_P$. R1866 denotes glass of pore radius R_P = 1866 Å, R893 is 893 Å, etc. Φ is the porosity.

accessible only through the smaller size (i.e., $R_P = R_1$). For this model, $2\sigma^{-1}/R_P = {}^4/_3$, as compared with 1.45 and 1.15 for glasses R893 and R1866. Thus, it should be kept in mind that the R_P values in Table II (which were adjudged more self-consistent and thus used in preference to $2\sigma^{-1}$) are smaller than the actual average R_P values and that, despite the apparently quite narrow pore size distributions of glasses R893 and R1866, variation in pore size by a factor of 2 or 3 (as is seen in micrographs of similar CPGs[36]) is not inconsistent with the characterization data. However, neither electron micrographs of similar CPGs[36] nor the small amounts (3–6%) of mercury trapped upon depressurization[41] indicates that there are many *severe* constrictions.

For glass R703, Haller provided a value of median R_P = 620 Å. Previously published mercury intrusion curves by Haller[40] (for a glass with R_P = 620 Å) indicate that he used $-\gamma_{Hg} \cos \theta_A \approx 324$ dyn/cm. Thus, for consistency, the supplied R_P was corrected to 703 Å.

Glass Pretreatment. The surfaces of these glasses were silanized to prevent adsorption of polymer, by reaction of surface-activated and thoroughly dried porous glass with a large excess of chlorotrimethylsilane in toluene.[41] The efficacy of this treatment was tested by adding a solution of polystyrene in 2-fluorotoluene to a sample of silanized, high-surface-area glass, under conditions providing about 60 Å^2 of surface per monomer unit. No polymer (or, at most, 7%, corresponding to uncertainty in the test method) was adsorbed on the silanized glass. Even *untreated* glass showed relatively low (ca. 30%) adsorption.

Dynamic Light-Scattering Experiments. Two light-scattering arrangements[27,28] were used: homodyne for bulk (unbounded) solution measurements and heterodyne for measurements in the porous glass. For these two arrangements, respectively, the measured photon count autocorrelation function $C(\mathbf{q},t)$ is given by[27,28]

$$C(\mathbf{q},t) = B\{1 + f_{HO}|g^{(1)}(\mathbf{q},t)|^2\} \quad (3a)$$

$$C(\mathbf{q},t) = B\{1 + f_{HE}|g^{(1)}(\mathbf{q},t)|\} \quad (3b)$$

where $\mathbf{q}$ is the scattering wave vector ($|\mathbf{q}| = q = \{4\pi n/\lambda_0\} \sin \{\theta/2\}$, with n the refractive index, λ_0 the wavelength in vacuo, and θ the scattering angle), t the delay time, $g^{(1)}(\mathbf{q},t)$ the normalized scattered electric field autocorrelation function, B the base line, f_{HO} the homodyne coherence factor, and f_{HE} the effective heterodyne coherence factor.

In the heterodyne arrangement, light scattered by the glass (stationary) serves as a strong local oscillator for mixing with light scattered by the polymer solution (about 100:1 intensity ratio). The two wave fronts are well matched since they originate in the same volume. The scattering from the glass was controlled by adjusting the refractive index of the solution by changing the temperature. Measurements were made at the same temperature (in the range 32–46 °C) for each pair of corresponding bulk and porous glass samples. This local oscillator scheme involves a tradeoff between the optimization of signal-to-noise and base-line determination and the minimization of homodyne contributions to the autocorrelation function.[41] In these experiments, the scattering volume was entirely within a single porous glass fragment; this eliminated any contribution from diffusion in bulk solution and thus the need to know the equilibrium partitioning coefficient.

A fairly standard light-scattering spectrometer was used. The source was a 50-mW Spectra-Physics 125 helium–neon laser, and detection was with photon-counting electronics. The cell-holder vat assembly had seven windows (scattering angles from 15° to 155°) with axes tilted 5° from the horizontal to lessen stray light. Neither polarizer nor analyzer was used. Two different Langley-Ford Instruments (Coulter Electronics) digital correlators were used: the 1096 Model, with 256 contiguous channels plus 16 channels reserved for a base line (these latter optionally delayed by $1024\Delta t$, with Δt the sample time), and the DC-64 Model, with 56 contiguous channels plus an 8-channel base line (optionally delayed by $64\Delta t$). These delayed channels proved to be absolutely essential for a reliable estimate of the true base line of heterodyne autocorrelation functions, as one would expect.[42]

Bulk solutions were run in the homodyne[27,28] mode. Correlation functions spanned about 4 decades of decay; that is, $2\langle\Gamma\rangle N_{LAST}\Delta t \approx 10$, with $\langle\Gamma\rangle$ the average decay rate, N_{LAST} the number of the

last contiguous channel, and Δt the sample time. Experiment durations provided $>1 \times 10^7$ counts above base line. The noise-to-signal, $N/S \approx (1 + f_{HO})^{1/2}/(f_{HO}B^{1/2})$, with B the base line, was less than ca. 8×10^{-4} for these homodyne experiments.

Corresponding heterodyne measurements had poorer signal-to-noise. For typical run times (about 1 h), $N/S \approx 1/(f_{HE}B^{1/2})$ was targeted at 3×10^{-3} and ranged from about 8×10^{-4} to 1×10^{-2}. Heterodyne correlation functions also spanned about 4 decades of decay, that is, $\langle\Gamma\rangle N_{LAST}\Delta t \approx 10$. The apparent coherence factor f_{HE} was targeted at 0.01–0.02 (actual f_{HE} was about 0.001–0.06, compared to f_{HO} values of 0.3–0.6), to provide a reasonable compromise between some homodyne contribution on the one hand and accurate determination of the base line and reasonable S/N on the other hand.[41] The local oscillator was controlled to give fractional amplitude of the homodyne term of about 0.005–0.025.

Data Analysis. Correlation functions $C(\mathbf{q},t)$ were analyzed by linear least-squares fits to a second-order cumulants expansion:[43]

$$\ln \{[C(j\Delta t) - B]/[C(k\Delta t) - B]\} = a + b(j\Delta t) + c(j\Delta t)^2 \quad (4)$$

with B the base line and k the first data channel used in the fit. The fitting parameters a, b, and c are related, respectively, to the coherence factor f_{HO} (or f_{HE}), the average decay rate $\langle\Gamma\rangle$, and the variance of the decay rate distribution μ_2.

Some data were also analyzed by inverse Laplace transform, using Provencher's CONTIN program,[44] to solve for the regularized, constrained nonnegative, and scaled (by f_{HE}) decay rate distribution $G(\Gamma)$. Starting with eq 3b, this method solves the following for $G(\Gamma)$:

$$\{C(j\Delta t)/B\} - 1 \cong \int_0^\infty G(\Gamma) \exp(-\Gamma j\Delta t)\, d\Gamma \quad (5)$$

The integrals in eq 5 were approximated by sums to obtain $G(\Gamma)$ at logarithmically spaced values of Γ; details have been given elsewhere.[41] Cumulants and Laplace inversion gave similar results, at least in the principal regions of interest (diffusion in bulk solution and at low wave vector in the porous glasses). However, for any given sample, systematic differences were seen, primarily because of base-line uncertainty and variation in the fraction of homodyne signal. Although the *direction* of this systematic difference was the same regardless of q for a given sample, it was random from sample to sample. Hence, most of the results presented in this paper were obtained from simpler second-cumulants fits.

Results and Discussion

Experimental Overview. We have examined diffusion in dilute solution for small ratios of polymer size to pore size $0.017 < \lambda_H < 0.47$, where $\lambda_H \equiv R_H/R_P$. Since the upper limit of λ_H only approaches the lower bound of scaling theory,[9] these results are for the change in dynamics of more or less spherical polymer coils with an increase in λ_H. (Neither the location nor the sharpness of the transition from dilute sphere to dilute confined chain behavior is precisely defined by the scaling theory but has only been given roughly[7,9] as $R_F/R_P > 2$, with R_F the polymer end-to-end distance, which translates to $R_G/R_P > 0.82$ or $\lambda_H > 0.56$.)

Despite obvious interest, light-scattering experiments at greater λ_H were impractical for two reasons: first, low signal (the equilibrium partitioning coefficient[9,33-35] approaches zero as λ_H increases) and, second, because of the requirement that $(\mathbf{q}\cdot\mathbf{R}_{G,\parallel}) < 1$ for translational diffusion to dominate the light-scattering spectrum. Given the R_P values of our glasses, polymers large enough to achieve large λ_H would violate this condition. Here $\mathbf{q}\cdot\mathbf{R}_{G,\parallel}$ is the projection of the longest dimension of the chain, assumed parallel to the pore direction, onto the scattering wave vector. This condition, the analogue of the usual condition $qR_G < 1$, was satisfied for most, but not all, samples.[41]

Diffusion Regimes. Wave Vector Dependence. By varying the scattering wave vector q, we have also examined the spatial dependence of diffusion, over a limited range of lengths. Three distinctly different diffusion "regimes" are observed. This wave vector dependence (Figures 2–4) is best considered in terms of the dimensionless variable qR_P, which is the ratio of pore size to the characteristic distance over which diffusion is examined, q^{-1}. qR_P thus relates to the extent of structural "averaging" in a given measurement. (Since the porous glasses are isotropic on the scale of the scattering volume, only the magnitude q of the wavevector $\mathbf{q}$ is important.) As qR_P varies, different manifestations of microscopic Brownian motion are seen. Strictly universal behavior for different polymers and porous materials as a function of qR_P is neither expected nor observed.

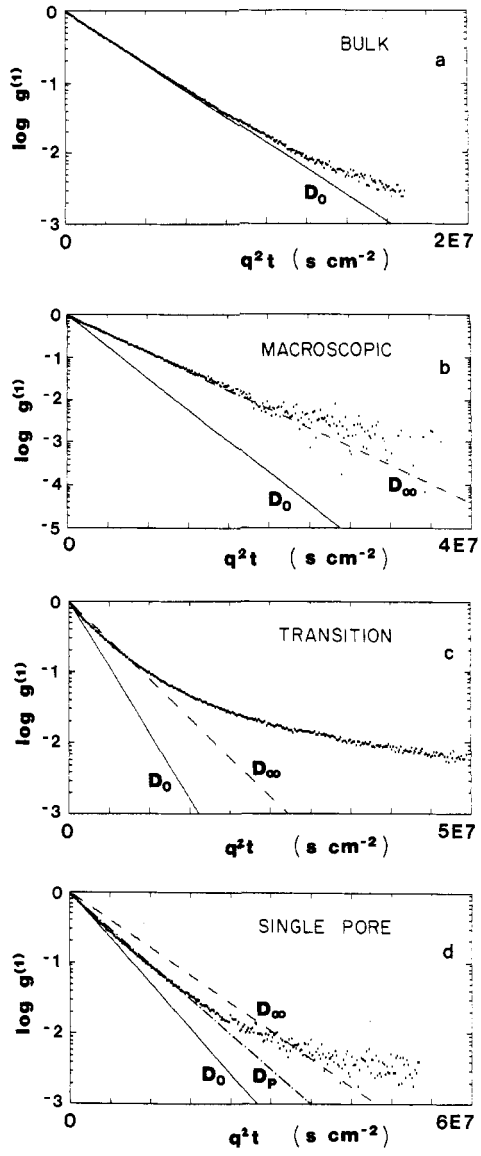

Figure 2. Four typical field correlation functions. Each measurement in porous glass (b–d) probes diffusion over a different distance relative to the pore radius, R_P. (a) Diffusion in bulk unbounded solution (shown for comparison). (b) Macroscopic diffusion regime, low qR_P ($qR_P = 0.35$). (c) Transition regime, intermediate qR_P ($qR_P = 1.85$). (d) "Single pore" diffusion regime, high qR_P ($qR_P = 5.3$). Parts a–c are for 181k polystyrene in glass R893 ($\lambda_H = 0.116$). Part d is for 406k polystyrene in glass R1866 ($\lambda_H = 0.090$).

Analysis of the wave vector dependence started from the general expression for the scattered electric field autocorrelation function $g^{(1)}(q,t)$:

$$g^{(1)}(q,t) = \int_0^\infty G(\Gamma,q) \exp(-\Gamma t)\, d\Gamma \quad (6)$$

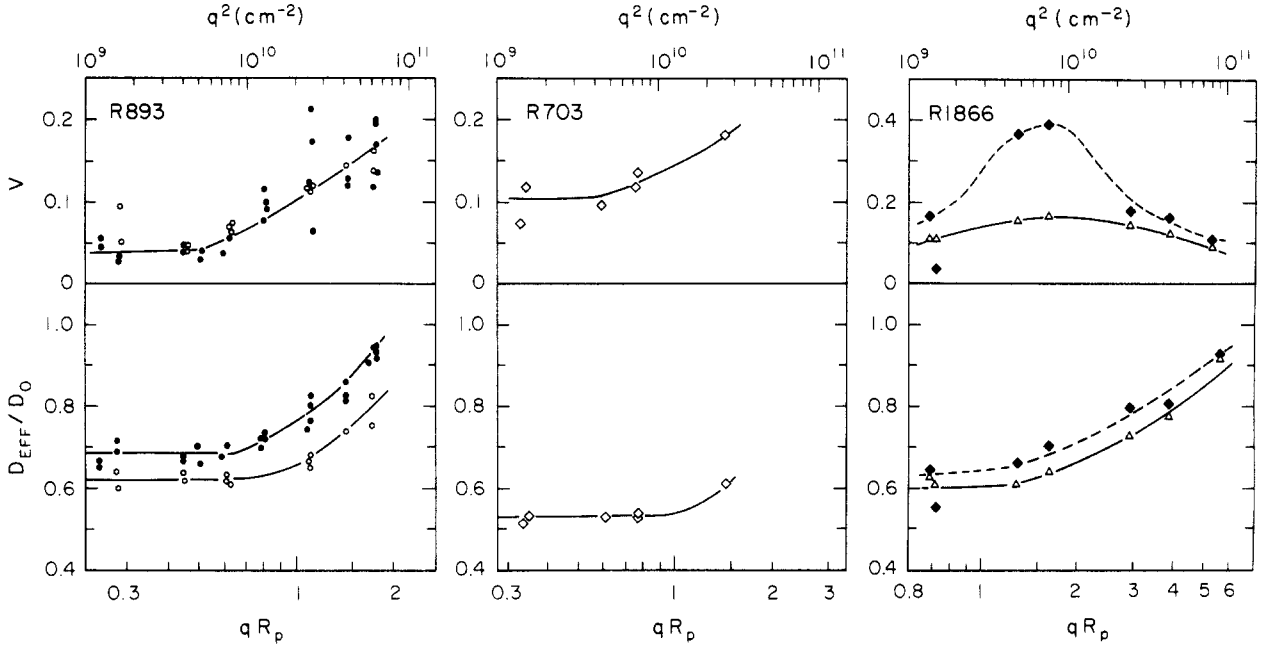

Figure 3. Wave vector dependence of the reduced average effective diffusion coefficient D_{EFF}/D_0 and of the normalized variance $V = \mu_2/\langle\Gamma\rangle^2$ of the decay rate distribution in three glasses: (left) glass R893, with 33k polystyrene ($\lambda_H = 0.044$, filled circles, Laplace inversion analysis) and with 102k PS ($\lambda_H = 0.084$, open circles, second-order cumulants analysis); (middle) glass R703, with 21k PS ($\lambda_H = 0.045$, second-order cumulants analysis); (right) glass R1866, with 406k PS ($\lambda_H = 0.090$), analyzed by Laplace inversion (diamonds) and second-order cumulants (triangles). Second cumulants are known to underestimate the variance of broad distributions. In the graph of D_{EFF}/D_0, lines at low qR_P were obtained from linear fits of $\langle\Gamma\rangle$ versus q^2 where $\langle\Gamma\rangle = D_{EFF}q^2$. Other curves show the trends of the data.

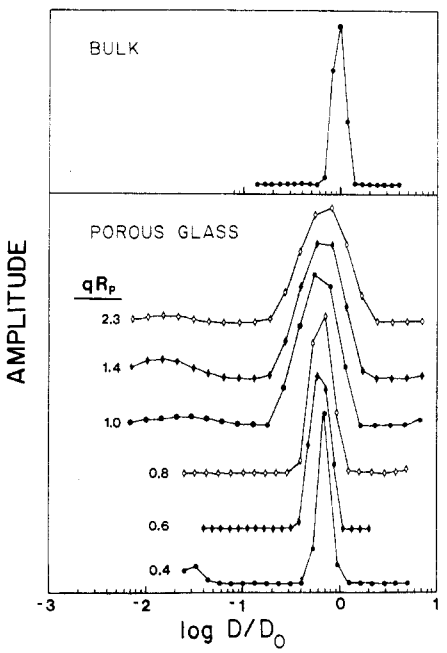

Figure 4. Decay rate spectra as a function of qR_P. Plotted are amplitude distributions (arbitrary units) of *apparent* decay rates normalized by the decay rate in bulk solution, $\Gamma/\langle\Gamma\rangle_0 = D/D_0$. These distributions were obtained by Laplace inversion by using Provencher's CONTIN program.[44] Data are for 33k polystyrene (R_H = 40 Å) in glass R893. The top spectrum shows the finite dispersity of the same polymer in bulk solution, while the rest show the narrowing and shifting of the decay rate distribution as the wave vector q decreases.

where $G(\Gamma,q)$ is the normalized distribution of the amplitudes of the generalized decay modes (relaxation times $1/\Gamma$) at wave vector q. The first moment of the distribution, $\langle\Gamma\rangle$, corresponds to some average *effective* decay rate for concentration fluctuations of wave vector q. The second moment of the distribution, μ_2, gives the breadth of the distribution of *apparent* decay rates. Usually, this variance is appropriately normalized as $V \equiv \mu_2/\langle\Gamma\rangle^2$. Corresponding to the average *effective* relaxation rate, $\langle\Gamma\rangle$, is a q-dependent effective diffusion coefficient D_{EFF}, which is defined by analogy to bulk solution as $D_{EFF} \equiv \langle\Gamma\rangle/q^2$. The ratio of this *effective* diffusion coefficient in the porous material to the diffusion coefficient in bulk solution, $D_{EFF}/D_0 \equiv \langle\Gamma\rangle/\langle\Gamma\rangle_0$, shows more clearly than $\langle\Gamma\rangle$ or D_{EFF} changes relative to bulk solution as a function of q, from sample to sample and from glass to glass.

The different diffusion regimes, in terms of qR_P, are illustrated by typical correlation functions (Figure 2), by plots of D_{EFF}/D_0 and V versus q^2 and qR_P for typical samples in the three different glasses (Figure 3), and by plots of $G(\Gamma/\langle\Gamma\rangle_0)$ versus $\Gamma/\langle\Gamma\rangle_0$ for different qR_P (Figure 4).

For the smaller pore size glasses (Figure 3, left and middle) both D_{EFF}/D_0 and V are constant at low qR_P and increase significantly at higher qR_P. This transition is at $qR_P \approx 0.7$–0.8 for D_{EFF}/D_0, but at a somewhat lower value $qR_P \approx 0.5$–0.6 for V. For the larger pore size glass (Figure 3, right), D_{EFF}/D_0 is relatively constant at low qR_P but increases significantly at higher qR_P, above $qR_P \approx 1.3$. The variance V has a maximum at $qR_P \approx 1.5$–2.0 and decreases for both lower and higher qR_P. As with the smaller pore size glasses, the value of qR_P below which D_{EFF}/D_0 is approximately constant is greater than the value of qR_P below which V is constant.

The macroscopic diffusion regime, at low qR_P (Figure 2b), shows behavior analogous to diffusion in bulk solution (Figure 2a). In both cases the average (essentially single) decay rate $\langle\Gamma\rangle$ of the correlation functions scales with q^2; D_{EFF} is constant. Correlation functions $g^{(1)}(q,t)$ for a given polymer and different (but small) q superpose when plotted versus q^2t. In bulk solution, D_{EFF} is the diffusivity D_0, while in the porous glass (low qR_P limit), D_{EFF} is identified as an effective macroscopic diffusion coefficient D_∞. The assertion that correlation functions at low qR_P are "single exponential" is based on the observation that V levels off at low qR_P at a similar, but slightly higher,

value than that in bulk solution (Figure 3). This is also illustrated in Figure 4, where the width of the shifted decay rate distribution at low qR_P is about the same as in bulk solution.

Correlation functions in the intermediate qR_P regime (Figure 2c) show a high degree of nonexponentiality even though the polymer is monodisperse. Further, correlation functions do not superpose when plotted versus q^2t. The initial decay rate is more rapid than in the macroscopic diffusion regime but less rapid than in bulk solution; however, at long times the correlation functions decay even more slowly than in the macroscopic diffusion regime, at equivalent values of q^2t. The increase in nonexponentiality with increase in q runs counter to the expected trend if this spectral broadening were caused by very slow relaxations or wave vector divergence.

The range of qR_P over which correlation functions are significantly nonexponential spans about 1 order of magnitude, $0.5 < qR_P < 5$, and is centered at $qR_P \approx 1.5$. This relatively narrow range observed for these porous glasses is further evidence, albeit indirect, that the structure of the pore space is reasonably uniform. For a porous material with a broader pore size distribution, nonexponential behavior of $g^{(1)}(q,t)$ would be expected over a wider range of qR_P. Nonexponential behavior is a manifestation of the non-Gaussian nature of the probability distribution function $P(\mathbf{R},t|0,0)$ for polymer displacements $\mathbf{R}$ in the porous material, due to the presence of reflecting walls (e.g., see ref 31). Given that $\mathbf{q}$ is conjugate to $\mathbf{R}$, the deviation from a Gaussian P and single-exponential $g^{(1)}(\mathbf{q},t)$ is expected to be a maximum for $q^{-1} \approx R_P$, as is indeed observed.

Data at the highest accessible qR_P values (Figure 2d) support the reasonable expectation that for $qR_P \gg 1$ (provided $qR_G < 1$) the decay rate is given by $\langle\Gamma\rangle \approx D_P q^2$, where D_P is the intrapore diffusivity, that is, D_0 as modified by polymer–wall hydrodynamic interactions, and also by any changes in monomer–monomer hydrodynamic interactions due to the polymer being confined.

The physical significance of the diffusion coefficients D_0, D_∞, and D_P differs. The subscript 0 in D_0 denotes diffusion in bulk (unbounded) solution at dilute but finite concentration, that is, without extrapolation to infinite dilution. The subscript ∞ in D_∞ denotes diffusion over macroscopic (i.e., essentially infinite) distances in the porous glass, whereas the subscript P in D_P denotes diffusion over short distances in the pore fluid. The coefficients D_0 and D_P are true diffusivities (insofar as the concentrations are sufficiently dilute that the measured mutual diffusion coefficients can be considered equal to the self-diffusion coefficients, or diffusivities); that is, D_0 and D_P are, to first order, related only to the hydrodynamic resistance encountered by diffusing polymer molecules. In contrast, D_∞ is not a diffusivity but instead is a phenomenological coefficient that incorporates extrahydrodynamic (e.g., structural) effects. (Similarly, the phenomenological diffusion coefficient measured in membrane transport experiments includes a factor of the partitioning coefficient and is not a true diffusivity.) The low qR_P behavior is consistent with the expectation that the decay of sufficiently long wavelength fluctuations, where structural variations should be effectively averaged, is governed by a single macroscopic relaxation rate. The necessary criterion for being able to use macroscopic forms of Fick's laws (which implies that there is a single macroscopic relaxation rate) to describe *transient* diffusion in a random porous material has been given as the requirement that diffusion be "quasi-steady" on a pore scale.[26] Applied to the *equilibrium* dynamic light-scattering experiment,[41] this translates to the requirement that the characteristic time τ_q associated with the relaxation of a concentration fluctuation of wavevector q, $\tau_q \approx (D_\infty q^2)^{-1}$, be much longer than the time between wall collisions, $t_{WALL} \approx R_P^2/D_P$. In other words, the longitudinal relaxation rate should be much slower than the transverse relaxation rate. This condition is satisfied in the limit of small qR_P.

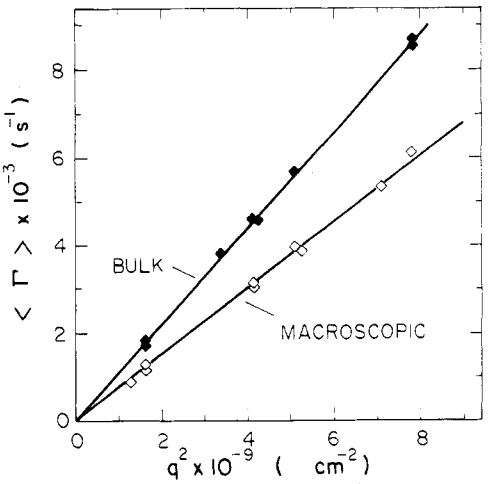

Figure 5. Typical plots of average decay rate $\langle\Gamma\rangle$ versus the square of the scattering wave vector q^2, as were used to obtain the coefficients for diffusion in bulk solution (D_0), and for macroscopic diffusion in a porous glass (D_∞). These data are for 33k polystyrene in glass R893 ($\lambda_H = 0.044$, $D_0 = 1.11 \times 10^{-6}$ cm^2/s and $D_\infty = 7.61 \times 10^{-7}$ cm^2/s).

We note that diffusion coefficients in bulk solution D_0 and for macroscopic diffusion in the porous glass D_∞ were obtained in the usual way, as the slope of linear fits of $\langle\Gamma\rangle$ versus q^2, over an appropriate range of q^2. Typical data and fitted lines are shown in Figure 5.

Concentration Dependence of Diffusion Coefficients. Quantitative comparisons between experiment and theory made later in this paper are based on diffusion measurements at finite concentration, not extrapolation of D_∞ and D_0 to infinite dilution. We show that by maintaining polymer concentration in the bulk fluid surrounding the porous fragment at a relatively constant fraction of the bulk solution overlap concentration ($c_0/c^* \sim 1/8$), it is reasonable to expect that the resulting uncertainty in D_∞/D_0 as a function of relative size, λ_H, is minimized.

An experiment to estimate systematic error in D_∞/D_0 was performed (401k polystyrene, glass R893, $\lambda_H = 0.185$). Analysis employed the reasonable assumption of linear concentration dependence:

$$D_0 = D_0^0(1 + k_{D,0}c_0) \quad (7)$$

$$D_\infty = D_\infty^0(1 + k_{D,G,0}c_0) \quad (8)$$

$$D_\infty = D_\infty^0(1 + k_{D,G,P}c_P) \quad (9)$$

where D_0 and D_∞ are measured mutual diffusion coefficients and where D_0^0 and D_∞^0 are self-diffusion coefficients. The concentrations in the fluid surrounding the glass fragment (c_0) and inside the pores (c_P) are related via the partitioning coefficient K_D as $c_P = K_D c_0$. The coefficient $k_{D,G,0}$ in eq 8 pertains to the easily measurable concentration c_0, but $k_{D,G,P}$ in eq 9 is with regard to the actual concentration c_P inside the pores (not directly measurable). Equations 7 and 8 are best fit by

$$D_0^0 = (2.62 \pm 0.02) \times 10^{-7} \text{ cm}^2/\text{s},$$
$$k_{D,0} = 70 \pm 4 \text{ cm}^3/\text{g}$$

$$D_\infty^0 = (1.18 \pm 0.02) \times 10^{-7}\ \mathrm{cm^2/s},$$
$$k_{D,G,0} = 186 \pm 20\ \mathrm{cm^3/g}$$

The stronger concentration dependence in the pores, where polymer motion is highly constrained, is expected. With the estimate $K_D \approx 0.5$–0.7 for $\lambda_H = 0.185$, the coefficient in eq 9, $k_{D,G,P}$ ($=k_{D,G,0}/K_D$), is 270–370 $\mathrm{cm^3/g}$, which is much higher than the corresponding quantity in eq 7, $k_{D,0}$.

With the exception of solutions prepared for this concentration-dependence study, all solutions in this work used $0.10 < c_0/c^* < 0.16$, with average $c_0/c^* = 0.12 \pm 0.02 \approx {}^1/_8$. Since c^* was estimated from $[\eta]$, eq 7 can be rewritten, for all other experiments, as

$$D_0/D_0^0 \approx 1 + \{k_{D,0}/8[\eta]\} \qquad (10)$$

Systematic change in D_0/D_0^0 as a function of molecular weight M is thus related to the molecular weight dependence of the quantity $k_{D,0}/[\eta]$. Huber et al.[46] (among others) have examined the dependence of k_D^* (a quantity proportional to $k_{D,0}/[\eta]$) on M for polystyrene in the good solvent toluene. On the basis of their results, $D_0/D_0^0 \approx 1.04$–1.08 for $M = 2 \times 10^4$–2×10^6 (the range of M in our experiments; see Table I), for measurements at $c_0/c^* \approx {}^1/_8$. This is a relative change in D_0/D_0^0 of only 4% over the entire range of molecular weight. The hydrodynamic radius, which we calculated from D_0 and not D_0^0, varies from $R_H/R_H^0 \approx 0.964$–0.925 over the corresponding range of M.

Corresponding theory is lacking for the dependence of D_∞/D_∞^0 (i.e., $k_{D,G,P}$) upon molecular weight M and the relative size parameter λ_H, preventing estimation of the systematic error in D_∞/D_∞^0. Systematic error in our dynamic light-scattering experiments would be determined by the molecular weight dependence of the quantity $k_{D,G,0}/[\eta]$. This reduced parameter is probably not an extremely strong function of λ_H and M, because as λ_H increases, the partitioning coefficient decreases. Therefore, although $k_{D,G,P}$ will be a strong function of M and λ_H, the product $k_{D,G,0} = K_D k_{D,G,P}$ will be much less so. Further, at large λ_H, $K_D \propto \exp(-\lambda_H^{5/3})$,[9] so $k_{D,G,P}$ would have to have exponential dependence on λ_H for $k_{D,G,0}$ to remain an increasing function.

It is noted that in other studies of polymer diffusion in porous materials, this aspect of the concentration dependence has heretofore always been ignored. (A quite different effect, that of concentration on partitioning, has been considered with regard to membrane transport coefficients.[14,18,47]) It can be seen, from both the ratio $(D_\infty/D_0)/(D_\infty^0/D_0^0) \approx 1.10$ for $c_0/c^* \approx {}^1/_8$ and the ratio $k_{D,G,0}/k_{D,0} \approx 2.65$, that this neglect of concentration dependence can lead to significant absolute and systematic error, even at the low (usually considered "dilute") concentrations used in these and other experiments such as transmembrane diffusion. In this work, an attempt has been made to remove the systematic concentration dependence by scaling initial solution concentrations to the overlap concentration.

Results of hindered diffusion experiments are generally plotted as a reduced diffusion coefficient versus a relative size parameter. In this work, as in previous membrane transport experiments, this involves plots of D_∞/D_0 versus λ_H (i.e., *not* D_∞^0/D_0^0 vs λ_H^0). Absolute and systematic error will affect the intercept and slope of such plots in ways that are readily apparent from the preceding discussion.[41] The concentration dependence of D_∞/D_0 and R_H may also in part explain discrepancies that have been observed among various membrane transport experiments.

Macroscopic Diffusion Coefficients. The ratio D_∞/D_0 versus the relative size parameter λ_H is plotted in Figure 7. Data for glasses R893 and R1866 fall on the same curve, whereas data for glass R703 differ, showing lower D_∞/D_0 values at a given λ_H. Interpretation of these results presumes that

$$D_\infty/D_0 = X_0 f(\lambda_H) \qquad (11)$$

where X_0 is the intrinsic conductivity of the porous glass for point particles, and $f(\lambda_H) \equiv D_P/D_0$ is the size-dependent ratio of the diffusivity inside the pores to that in bulk solution.

The factor X_0 ($1/X_0 = T_0$ is commonly called the tortuosity) arises in treatments of macroscopic diffusion in

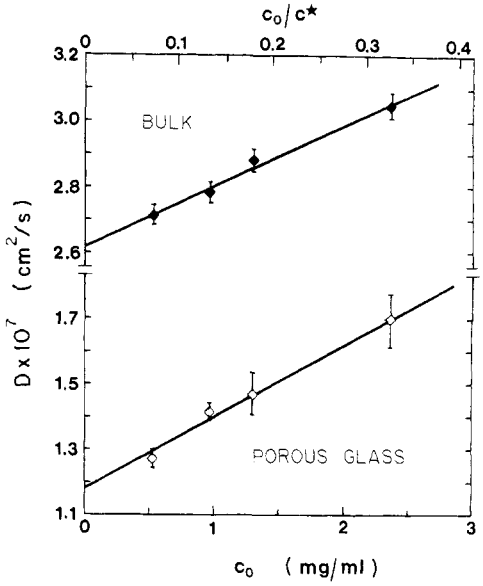

Figure 6. Concentration dependence of mutual diffusion coefficients, in unbounded (bulk) solution and in solution inside a porous glass. These data are for 401k polystyrene in glass R893. The abscissa is shown both as the concentration in bulk solution (c_0) and as c_0/c^*, with $c^* \approx 7.21$ mg/mL the overlap concentration in bulk solution. Lines are linear fits to the data.

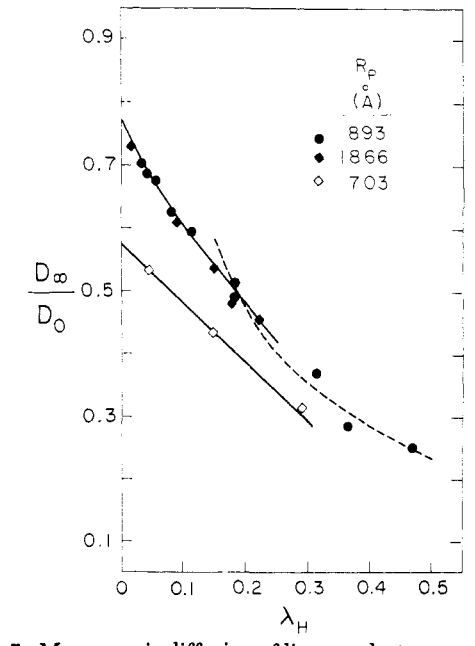

Figure 7. Macroscopic diffusion of linear polystyrenes in porous glasses. D_∞ is the macroscopic diffusion coefficient in the glass, D_0 is the diffusivity in bulk solution, and λ_H is the ratio of polymer hydrodynamic radius R_H to pore radius R_P. The solid curve through the data for glasses R893 and R1866 is a fit of low λ_H data to eq 13; the dashed curve through the same data is a fit of high λ_H data to the scaling prediction (eq 14). The solid line through the data for glass R703 is drawn through the first two points.

porous media,[24-26] where invariably the diffusant is implicitly assumed to be vanishing small relative to the pore size ($\lambda_H \to 0$), so that hydrodynamic (or other size-dependent) effects are negligible ($f \to 1$). In these theories, the value of D_∞/D_0 is determined solely by the geometry of the pore space, that is, factors such as geometrical tortuosity, constrictions, dead-end pores, fractal dimensions plus cutoff lengths, and the like.

The function f incorporates the effects of hydrodynamic interactions for particles of size comparable to the pores. For rigid particles, there are strong hydrodynamic interactions between particles and walls; additionally for flexible polymers, the polymer configuration can also change, thereby affecting frictional properties. Explicit expressions for f have been obtained for diffusion in single pores of ideal geometry.[2-8] These calculations and the track-etched membrane transport experiments to which they have been applied[10-18] correspond to the situation $X_0 = 1$, that is, no significant tortuosity.

The relation given by eq 11 is thus an ad hoc modification, to account for finite size, of the corresponding result for macroscopic diffusion of point particles. The underlying assumption, that the structural and hydrodynamic effects are separable, is expected to be valid *only* if the pore space is "well-connected", with reasonably uniform pore size and with few severe constrictions.[41] Otherwise and more generally, the two effects will be *intimately linked* in the effective macroscopic diffusion coefficient D_∞. Heuristic but imprecise arguments to this effect are that the intrinsic conductivity will depend on diffusant size for a non-well-connected porous material, because constrictions present a size-dependent energetic hindrance to diffusion: as one increases the size of the diffusant in a given porous material, the relative "constrictedness" along a given path increases and molecules will also on the average take more "geometrically tortuous" paths. Therefore, inappropriate application of eq 11 to a non-well-connected (e.g., fractal) pore space can lead to wrong or misleading conclusions as to the causes of an overall hindrance to diffusion. Our use of eq 11 thus rests on the assumption that the three porous glasses have well-connected pore structures. This is reasonable insofar as the pore size distributions of these glasses are narrow and as there is no evidence for a significant number of severe constrictions.

The effective diffusion coefficient D_∞, which is measured by dynamic light scattering, includes neither the equilibrium partitioning coefficient (K_D) per se nor the porosity Φ. This is supported by the observations that (1) data for glasses R893 and R1866, which have different porosities, superimpose and (2) inclusion of Φ in D_∞ would imply intrinsic conductivity $X_0 > 1$ (or tortuosity $T_0 < 1$), an unphysical result.

Comparison to Theories for Hindered Diffusivity. The data were fit according to eq 11, using three expressions for $f(\lambda_H)$:

$$f_{CL}(\lambda_S) = 1 - 2.10444\lambda_S + 2.08877\lambda_S^3 - 0.94813\lambda_S^5 - 1.372\lambda_S^6 + 3.87\lambda_S^8 - 4.19\lambda_S^{10} + \ldots \quad (12)$$

$$f_{BG}(\lambda_S) = \frac{1 + \frac{9}{8}\lambda_S \ln \lambda_S - 1.539\lambda_S + O(\lambda_S)}{(1 - \lambda_S)^2} \quad (13)$$

$$f_S(\lambda_H) = \xi\lambda_H^\gamma, \quad \gamma = (n-1)/n \quad (14)$$

Equations 12 and 13 (applicable at small λ's) describe the diffusion of hard spheres in cylindrical pores and are based on low Reynolds number hydrodynamics (see ref 1, 2, and 5 for reviews). Equation 12 is based on the rather dubious[2] center-line approximation and expresses the diffusivity reduction as a power series in λ_S, where λ_S is the ratio of the sphere radius to pore radius. (For the range of our data, this expression should be as good as more exact center-line solutions.[1,5]) Equation 13 was obtained by Brenner and Gajdos,[4] taking into account the radial dependence of the friction factor; Anderson and Quinn[3] had numerically calculated a nearly identical result previously. Their theory is claimed applicable for $\lambda_S \ll 1$ or, as alternatively stated, $\lambda_S \leq 0.1$.[4]

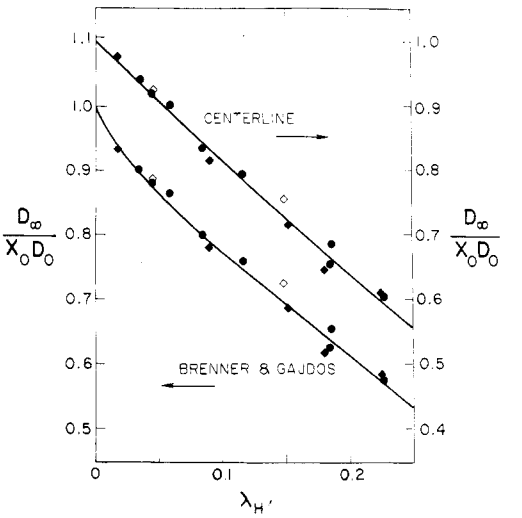

Figure 8. Comparison of low λ_H data to theories for diffusion of hard spheres in cylindrical pores. Upper curve (right-hand ordinate scale): fit to center-line theory (eq 12). Lower curve (left-hand scale): fit to Brenner–Gajdos theory (eq 13). The ordinate (D_∞/X_0D_0) corresponds to the function $f(\lambda_H) = D_P/D_0$ in the text. The curves correspond to $f_{CL}(\lambda_S) = f_{CL}(\kappa\lambda_H)$ and $f_{BG}(\lambda_S) = f_{BG}(\kappa\lambda_H)$ for the center-line and Brenner–Gajdos fits respectively; X_0 and κ were adjustable parameters in each fit. Data from glasses R893 (circles) and R1866 (filled diamonds) were included in the fit; data from glass R703 (open diamonds) are shown but were not included in the fits.

Equation 14 is based on scaling arguments[6-8] for the diffusion of strongly confined chains (large λ_H), in a good solvent, *in isolated regular pores of any geometry*. In that expression, ξ is an unknown numeric factor, and n is the exponent in the relation $R_H \propto M^n$. This is a slight generalization of the result for ideally good solvents ($\gamma = -^2/_3$),[6-8] with the reasonable assumption that the basic scaling arguments are valid for a less than ideally good solvent ($^1/_2 \ll n < {}^3/_5$).

Fits to eq 12 and 13, which rest on the assumption that the diffusion of flexible polymers that are small compared to the pore size can be modeled as the diffusion of hard spheres, involve two adjustable parameters: the intrinsic conductivity X_0 and a scaling factor κ relating the relative size parameter λ_H, to λ_S in $f_{CL}(\lambda_S)$ and $f_{BG}(\lambda_S)$:

$$\lambda_S = \kappa\lambda_H \quad (15)$$

For all glass R893 and R1866 data with $\lambda_H \leq 0.23$, a fit to the Brenner–Gajdos theory yields $X_0 = 0.781 \pm 0.006$ and $\kappa = 0.76 \pm 0.02$, while a fit to the center-line theory yields $X_0 = 0.748 \pm 0.006$ and $\kappa = 0.88 \pm 0.02$. The parameters X_0 and κ from the two fits differ in the expected way. (Over this range of λ_H, a linear fit gives nearly identical results: $X_0 = 0.744 \pm 0.006$ and $\kappa = 0.85 \pm 0.05$.) The corresponding center-line estimates for glass R703, from the two data points with the lowest λ_H, are $X_0 = 0.58$ and $\kappa = 0.78$.

Using the values of X_0 and κ from these fits, values of $f(\lambda_H) = D_\infty/D_0X_0 = D_P/D_0$ were calculated and compared to the functions $f_{CL}(\kappa\lambda_H)$ and $f_{BG}(\kappa\lambda_H)$ (Figure 8). Sig-

nificantly, data from all three glasses fall on the same curve, which indicates (1) that the pore sizes R_P are correct on a relative basis and, more importantly, (2) that the separation of intrinsic conductivity and hydrodynamic interactions as represented by eq 11 is justified for these porous glasses. Although the data for glasses R893 and R1866 are fit by both the center-line and Brenner–Gajdos theories to within the measurement uncertainty, the Brenner–Gajdos theory must be considered as having a more realistic and rigorous theoretical basis.

It is impossible to assign any definite and unambiguous meaning to the parameter κ or, in other words, to precisely address the question of which flexible polymer radius corresponds to the effective hard-sphere radius to be used in the theories for reduced diffusivity. First and most importantly, there is uncertainty in both the absolute magnitude of the normal pore radius R_P from mercury porosimetry and in the relationship of this R_P to the actual pore space geometry (see the Experimental Section). Second, the pore diffusivity D_P will be some weighted average over the poorly known distribution of pore sizes; however, given the narrow pore size distributions, this effect will be relatively unimportant. Third, the exact numerical coefficients appropriate to use in eq 12 and 13, given the complicated geometry of these porous glasses, are not known, although they should not differ greatly from those for cylindrical pores.[48]

The result that $\kappa < 1$ could be due simply to underestimation of R_P by mercury porosimetry. (Certainly, however, the data show that R_P values are correct in at least a relative sense.) This interpretation would imply that the R_P values used in calculating λ_H were about 10–25% too low, which is in agreement with the estimates of the undervaluation of R_P based on the hydraulic radii σ^{-1} (Table II), which indicate R_P values ca. 15–45% too low. If this argument is correct, then the agreement between the experimental data for $f(\lambda_H)$ and the theory for $f_{BG}(\lambda_S)$ is very good, with the identification of the appropriate effective hard-sphere radius as the hydrodynamic radius of the flexible polymer, that is, $\kappa \cong 1$ and $\lambda_S \cong \lambda_H$. This conclusion is in apparent conflict with results of previous membrane transport experiments (the interpretation of which, however, requires knowledge of the equilibrium partitioning coefficient),[13-18] in particular that of a comparative study of linear versus star polyisoprenes.[17]

It is important to ask over what range of the relative size parameter λ_H it is reasonable to model the diffusion of flexible polymers as the diffusion of hard spheres. As λ_H increases, there will be a transition in the *hydrodynamics* from non-free-draining behavior ($D_P \propto M^{-3/5}$), where the polymer can be considered as a hard sphere, to free-draining (i.e., Rouse) behavior ($D_P \propto M^{-1}$) due to screening of intramolecular hydrodynamic interactions by the pore wall. However, the macroscopic diffusion coefficient D_∞ is not determined by hydrodynamics alone. The reptation result, $D_\infty \propto M^{-2}$, is obtained if the porous material consists of long one-dimensional objects (e.g., other polymer chains)[8] or three-dimensional objects in a periodic array.[49] For diffusion in a random porous material, the molecular weight dependence of D_∞ is expected to be even stronger than that given by reptation,[49] undoubtedly a consequence of strong partitioning effects that are negligible in a regular (i.e., well-connected) porous material. Clearly, the simple description of eq 11 is invalid for both these cases. Equation 11, with f given by the scaling result of eq 14, would be expected to hold only for strongly confined (Rouse) chains in a well-connected porous material *if* the distance between pore junctions were much larger than the extended length of the chains; in such a case, the pores would essentially be isolated, and $D_\infty \propto M^{-1}$ would be predicted. The crossover from Rouse to reptation dynamics for confined chains has been considered.[50]

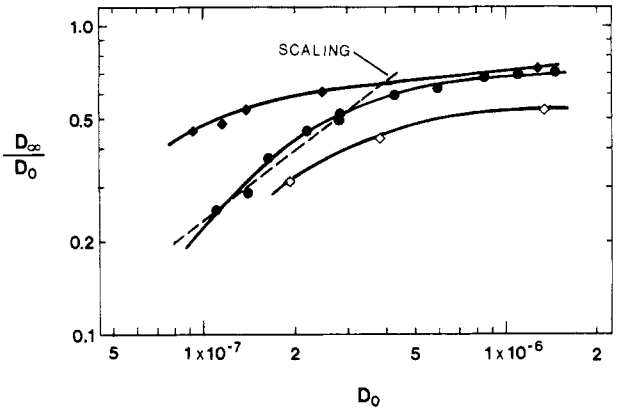

Figure 9. Plot of D_∞/D_0 vs D_0 for all three glasses: R893 (circles), R1866 (filled diamonds), and R703 (open diamonds). The slope of this plot is related to the molecular weight scaling exponents of D_∞ and D_0:$D_\infty \propto M^{-m}$ and $D_0 \propto M^{-n}$, and slope = $(m - n)/n$. The plateau at higher D_0 (lower M) can be interpreted as the behavior of non-free-draining ($m \approx n$) polymer coils, where the small decrease with increasing M is attributed to hydrodynamic interactions of these "hard spheres" with the walls. The more rapid decrease at lower D_0 (higher M) can be interpreted as free draining or perhaps even stronger dependence on molecular weight. The dashed line has the slope 0.75, predicted by scaling arguments (eq 14) for $m = 1$, $n = 0.57$.

Our data are consistent with a transition from non-free-draining to free-draining behavior at $\lambda_H \approx 0.15$–0.30. Even at these relatively low λ_H values, it is possible that screening of intramolecular hydrodynamic interactions is significant. We cannot rule out the alternative that the stronger λ_H dependence of D_∞/D_0 at higher λ_H is simply due to increasingly strong hydrodynamic interactions (not described by the center-line theory or the Brenner–Gajdos theory) of an essentially non-free-draining polymer coil with the walls. Unfortunately, we were unable to directly measure D_P to resolve this question, since, for these porous glasses, the conditions $qR_P \gg 1$ and $qR_G < 1$ could not be simultaneously satisfied at higher λ_H.

Our data indicate that the molecular weight dependence at the largest λ_H is stronger than $D_\infty \propto M^{-1}$ and is becoming stronger still at higher λ_H (i.e., that the slopes in Figure 9 are steeper with decreasing D_0). This may indicate a transition in the *macroscopic* diffusion behavior toward reptation dynamics or even toward the stronger dependence seen for random porous materials.[49] The dashed line in Figure 9 has the slope 0.75, which would be expected for free-draining behavior in isolated pores (eq 14) based on the exponent $n = 0.57$ in the relation $D_0 \propto M^{-n}$. As is reasonable for these porous glasses in which the pores are highly interconnected, there is no evidence for an extended Rouse-like regime ($D_\infty \propto M^{-1}$) as would be expected for diffusion in isolated pores of simple geometry.

Characterization of these glasses and the results for diffusion at small λ_H both indicate that the pore spaces are fairly regular, which might be expected to lead to reptation. We were not able to determine the molecular weight dependence of D_∞ in the limit $M \to \infty$, because of limitations on extending these light-scattering experiments to higher molecular weight. Such measurements might be possible by forced Rayleigh scattering.

Intrinsic Conductivity of the Porous Glasses. Values of the intrinsic conductivity X and the related quantities tortuosity T ($T = 1/X$) and formation factor F ($F = T/\Phi = 1/X\Phi$)[24,25] are given in Table II. (The

subscript 0, denoting point particles, is dropped). Numerous notational variations and even different definitions can be found in the literature for these quantities; all values in this paper follow the conventions just given.

Intrinsic conductivities of these glasses are relatively high, which is expected because of the high porosities and fairly uniform pore spaces. The lower intrinsic conductivity for R703 (lowest Φ), relative to R893 and R1866, is in accord with the generally expected correlation of X with Φ.

All the intrinsic conductivities are significantly higher than those previously reported for controlled pore glasses of similar Φ (see the following section). Otherwise, these values are in reasonable accord with experimental and theoretical values for "similar" porous materials;[24,25,51] for example, packings of spheres[24,25] ($\Phi \approx 0.4$) have $X \approx {}^3/_5$, and loose packs of sand[24,25] have relatively high $X \approx {}^2/_3$. Models of "normal" porous materials[24,25,51,52] predict ${}^1/_3 \leq X \leq 1$, although models can easily be envisioned that result in arbitrarily small X (e.g., fractal models[53]). While for randomly oriented *thin* pores, $X = \langle 1/\cos^2\theta \rangle^{-1} = {}^1/_3$ (the lower limit above), most real porous materials have "pores" with low aspect ratio; since flux lines can "cut across" such pores, $X > {}^1/_3$ is generally expected, with higher aspect ratio pores producing lower X. The following formula,[52] which allows for "shortcut" paths across pores and which has the "classic" limits, that is, $X = {}^1/_3$ ($T = 3$) for $\Phi \to 0$ and $X = 1$ ($T = 1$) for $\Phi \to 1$

$$X = 1 - {}^2/_3(1 + \Phi)(1 - \Phi)^{3/2} \qquad (16)$$

yields 0.83 (R893), 0.75 (R1866), and 0.61 (R703), which fall near our experimental X_0 values in Table II.

A significant result is that the porous glasses R893 and R1866, which have different porosities and pore sizes, have the same intrinsic conductivity. A number of theoretical and empirical expressions giving X as a unique and single-valued function of Φ have been proposed, despite overwhelming evidence to the contrary (e.g., see ref 24, 25, 51, and 52). Our result adds to the evidence that no universal relation of X as a function of Φ exists.

Comparison with Previous Experiments. Our dynamic light-scattering results are in essential agreement with those for diffusion of flexible polymers through track-etched membranes:[13-18] the results of both types of experiments are consistent with both hard-sphere and flexible-polymer-hindered diffusion theories, given the adjustable parameters in those theories.

However, our results conflict with those of previous studies of polystyrene diffusion in porous glasses.[19-22] We find that diffusion is in no way unusual; the ratio D_∞/D_0 decreases monotonically with increase in λ_H. Further, we find higher intrinsic conductivities, or lower tortuosities (by a factor of 2–5). It is suggested that the significantly lower and essentially constant effective diffusivities that have previously been observed may be due to a large boundary layer resistance.

Consider first those experiments involving transient diffusion of polystyrenes into controlled pore glasses. The lower molecular weight data ($\lambda_H < 0.4$) of Tennikov et al.,[20] *after* correcting for obviously erroneous D_0 values, are at least roughly consistent with our results, both in terms of D_∞/D_0 vs λ_H and in terms of the intercept at $\lambda_H = 0$. However, our data show no support for their conclusions that D_∞/D_0 can exceed unity or for extremal behavior—a minimum—in the dependence of D_∞/D_0 on λ_H. We also find no support for the conclusions of Colton et al.[19] that flexible polystyrenes have reduced effective diffusivities D_∞/D_0 that are independent of the relative size parameter λ_H (i.e., independent of molecular weight) in any given pore size glass (which they erroneously called free-draining). To the contrary, we find D_∞/D_0 to be a monotonically and significantly decreasing function of λ_H.

Similarly, our results are in substantial disagreement with those of Klein and Grüneberg,[22] who obtained diffusion coefficients of polystyrenes in porous glasses from size exclusion chromatography peak broadening. (N.B. There are significant numerical uncertainties in extracting D_∞ from SEC experiments, which may account for some of the disagreement.) For chromatographic partitioning coefficients $K_C > 0.35$, corresponding roughly to $\lambda_H < 0.25$, they found D_∞/D_0 independent of molecular weight (a finding similar to that of Colton et al.[19]). This can be contrasted to our results, where ca. 50% reduction in D_∞/D_0 is seen at $\lambda_H = 0.25$ relative to D_∞/D_0 at $\lambda_H = 0$. However, for $K_C < 0.35$ ($\lambda_H > 0.25$) they did observe size-dependent reductions in D_∞/D_0. This value of $K_C \approx 0.35$ corresponds to $\lambda_H \approx 0.25$, which from our results is tentatively identified as the λ_H, where transition to free-draining behavior occurs. It is possible that only when D_∞/D_0 assumes a stronger dependence on λ_H (regardless of the reason) is the SEC peak broadening technique sensitive enough to detect changes in D_∞/D_0.

Tortuosities found by Colton et al.[19] and by Klein and Grüneberg,[22] for controlled pore glasses of comparable porosity as those used in our work, are significantly higher and in disagreement with tortuosities found here. Colton et al. found $T = 2.9$, 2.3, 3.1, and 3.5 for $\Phi = 0.54$, 0.70, 0.58, and 0.60; Klein and Grüneberg obtained $T = 7.1$, 6.3, and 4.3 for $\Phi = 0.48$, 0.64, and 0.76. These are compared with our results of $T = 1.3$, 1.3, and 1.7 for $\Phi = 0.72$, 0.62, and 0.46. Perhaps the most reasonable explanation for the lower and essentially constant (i.e., molecular weight independent) D_∞/D_0 values observed in these previous studies would be a large boundary layer resistance[54] (which was assumed to be negligible and which also was not included in the theory of SEC peak broadening) in series with the diffusive resistance of the porous glass. Only at high molecular weights might the actual intraglass diffusional resistance become larger and dominate.

It is worth noting that, in other work[13,14] where the scaling theory has been considered, the hard-sphere and scaling theory fits to the data cross at values of $\lambda_H \approx 0.15$–0.30. This is the same as the value where the fits to our data cross. Although this may merely indicate that the scaling theory is incapable of fitting data at low λ_H (≤ 0.25 say, where the dependence of D_∞/D_0 upon λ_H is nearly linear), it also lends some support to the tentative identification in our work of this value of λ_H as the transition from non-free-draining to free-draining behavior.

Dynamic light-scattering experiments can potentially provide a more critical test of scaling theories and this transition in hydrodynamic behavior than can membrane transport experiments. These latter infer scaling behavior on the basis of a two-parameter fit, *of a power law times an exponential*, to the experimental data for a membrane diffusion coefficient $D_M/D_0 = K_D f(\lambda_H)$. Light scattering, in contrast, allows one to directly look for the hindered diffusivity power law, because the equilibrium partitioning coefficient K_D does not directly enter the effective diffusion coefficient that is measured.

Our interpretation of the fits of our data at low λ_H, where hard-sphere diffusion theories may be a reasonable approximation for flexible polymers, indicates that the appropriate hard-sphere radius to use in these theories is the hydrodynamic radius, that is, with a factor κ (see eq 15) of about unity. (This is after accounting for the effect of pore polydispersity.) This is to be contrasted with previous

conclusions of $\kappa = 1.45$,[13] or κ significantly less than 1,[15-17] from experiments on track-etched membranes. The higher result of Cannell and Rondelez[13] may be due to neglect of boundary layer resistance (estimated by them to be as high as 20%); to fit a low apparent D_M (i.e., including boundary layer resistance) would require a larger κ. Porosity, often poorly known in membrane transport experiments (e.g., extracted by assuming a Renkin center-line equation fit[14]), can similarly affect κ; as with K_D, the porosity does not enter the effective diffusion coefficient from light scattering. Nonetheless, it is difficult to reach any definitive conclusion about the exact "correct" flexible polymer radius to use in hard-sphere-hindered diffusion theories, because of nagging numerical details in both light-scattering and membrane diffusion experiments.

Conclusions

Dynamic light scattering has been used to measure directly the mutual diffusion coefficient of linear polystyrenes in three different porous glasses under conditions of macroscopic equilibrium. The macroscopic diffusion coefficient D_∞, which does not include the effects of equilibrium partitioning, is obtained from measurements at low wave vector, or more precisely, low qR_P. Contrary to previous results for diffusion of polystyrene in porous glasses, our results for the molecular weight dependence of the diffusion coefficient in these materials which have highly interconnected pore spaces is in no way unusual. This molecular weight dependence is entirely consistent with theories for the increased hydrodynamic drag for polymer diffusing in pores, which predict reduced intrapore diffusivities D_P relative to the diffusivity in bulk solution D_0 as a function of the relative size of polymer to pore λ_H. Our results are thus also consistent with previous experiments for diffusion of flexible polymers in track-etched membranes. We find universal behavior for D_P/D_0 versus λ_H for the three glasses which have different porosities and pore sizes. However, the *overall* reduction in the diffusion coefficient D_∞/D_0 versus λ_H is not universal but depends on the porous glass structure, through the intrinsic conductivity or tortuosity, in addition to the relative size λ_H. For these data, the structural and hydrodynamic effects are separable, due to the narrow pore size distribution of these glasses. Measured intrinsic conductivities are consistent with values for similar materials and also values calculated from reasonable structural models. The concentration dependence of the diffusion coefficient in the porous glass has been found to be much stronger than the concentration dependence in bulk solution.

Acknowledgment. We thank Professors R. Guyer, M. Muthukumar, and J. Machta for many useful discussions providing valuable insights into the problem at hand. We also thank Dr. N. Easwar for experimental assistance and Dr. W. Haller of the National Bureau of Standards for kindly providing one of the porous glass samples. The support of this work by the U. S. Air Force Office of Scientific Research under Contract No. AFOSR 84-0033 is gratefully acknowledged.

Registry No. Polystyrene, 9003-53-6.

References and Notes

(1) Happel, J.; Brenner, H. *Low Reynolds Number Hydrodynamics*; Prentice-Hall: Englewood Cliffs, NJ, 1965.
(2) Bean, C. P. In *Membranes: A Series of Advances*; Eisenman, G., Ed.; Marcel Dekker: New York, 1972; Vol. 1, p 1.
(3) Anderson, J. L.; Quinn, J. A. *Biophys. J.* **1974**, *14*, 130.
(4) Brenner, H.; Gajdos, L. J. *J. Colloid Interface Sci.* **1977**, *58*, 312.
(5) Paine, P. L.; Scherr, P. *Biophys. J.* **1975**, *15*, 1087.
(6) Brochard, F. *J. Phys. (Les Ulis, Fr.)* **1977**, *38*, 1285.
(7) Brochard, F.; de Gennes, P.-G. *J. Chem. Phys.* **1977**, *67*, 52.
(8) de Gennes, P.-G. *Scaling Concepts in Polymer Physics*; Cornell University Press: Ithaca, NY, 1979.
(9) Daoud, M.; de Gennes, P. G. *J. Phys. (Les Ulis, Fr.)* **1977**, *38*, 85.
(10) Beck, R. E.; Schultz, J. S. *Biochim. Biophys. Acta* **1972**, *255*, 273.
(11) Conlon, T.; Craven, B. *Aust. J. Chem.* **1972**, *25*, 695.
(12) Malone, D. M.; Anderson, J. L. *Chem. Eng. Sci.* **1978**, *33*, 1429.
(13) Cannell, D. S.; Rondelez, F. *Macromolecules* **1980**, *13*, 1599.
(14) Guillot, G.; Léger, L.; Rondelez, F. *Macromolecules* **1985**, *18*, 2531.
(15) Deen, W. M.; Bohrer, M. P.; Epstein, N. B. *AIChE J.* **1981**, *27*, 952.
(16) Bohrer, M. P.; Patterson, G. D.; Carroll, P. J. *Macromolecules* **1984**, *17*, 1170.
(17) Bohrer, M. P.; Fetters, L. J.; Grizzuti, N.; Pearson, D. S.; Tirrell, M. V. *Macromolecules* **1987**, *20*, 1827.
(18) Guillot, G. *Macromolecules* **1987**, *20*, 2600, 2606.
(19) Colton, C. K.; Satterfield, C. N.; Lai, C.-J. *AIChE J.* **1975**, *21*, 289.
(20) Tennikov, M. B.; Belen'kii, B. G.; Nesterov, V. V.; Anan'eva, T. D. *Colloid J. USSR* **1979**, *41*, 526.
(21) Giddings, J. C.; Bowman, L. M., Jr.; Myers, M. N. *Macromolecules* **1977**, *10*, 443.
(22) Klein, J.; Grüneberg, M. *Macromolecules* **1981**, *14*, 1411.
(23) Bishop, M. T.; Langley, K. H.; Karasz, F. E. *Phys. Rev. Lett.* **1986**, *57*, 1741.
(24) Bear, J. *Dynamics of Fluids in Porous Media*; American Elsevier: New York, 1972.
(25) Dullien, F. A. L. *Porous Media: Fluid Transport and Pore Structure*; Academic: New York, 1979.
(26) Lehner, F. K. *Chem. Eng. Sci.* **1979**, *34*, 821.
(27) Chu, B. *Laser Light Scattering*; Academic: New York, 1974.
(28) Berne, B. J.; Pecora, R. *Dynamic Light Scattering: With Applications to Chemistry, Biology, and Physics*; Wiley: New York, 1976.
(29) Cummins, P. G.; Staples, E. J. *J. Phys. E: Sci. Instrum.* **1981**, *14*, 1171.
(30) Hurd, A. J.; Mockler, R. C.; O'Sullivan, W. J. In *Proceedings from the 4th International Conference on Photon Correlation Techniques in Fluid Mechanics*; Mayo, W. T., Jr., Smart, A. E., Eds.; Joint Institute for Aeronautics and Acoustics, Stanford University: Stanford, CA, 1980; pp 22-1 to 22-10.
(31) Lan, K. H.; Ostrowsky, N.; Sornette, D. *Phys. Rev. Lett.* **1986**, *57*, 17.
(32) Phillies, G. D. J. *Macromolecules* **1986**, *19*, 2367.
(33) Casassa, E. F.; Tagami, Y. *Macromolecules* **1969**, *2*, 14.
(34) Giddings, J. C.; Kucera, E.; Russell, C. P.; Myers, M. N. *J. Phys. Chem.* **1968**, *72*, 4397.
(35) Doi, M. *J. Chem. Soc., Faraday Trans. 2* **1975**, *71*, 1720.
(36) (a) Haller, W. *Nature (London)* **1965**, *206*, 693. (b) Haller, W. *J. Chem. Phys.* **1965**, *42*, 686. (c) Haller, W.; Macedo, P. B. *Phys. Chem. Glasses* **1968**, *9*, 153.
(37) Adamson, A. W. *Physical Chemistry of Surfaces*, 4th ed.; Wiley-Interscience: New York, 1982.
(38) *Powder Technol.* **1981**, *29*. This entire issue is devoted to mercury porosimetry.
(39) Liabastre, A. A.; Orr, C. *J. Colloid Interface Sci.* **1978**, *64*, 1.
(40) Haller, W. *J. Chromatogr.* **1968**, *32*, 676.
(41) Bishop, M. T. Ph.D Thesis, University of Massachusetts, Amherst, MA, 1987.
(42) Oliver, C. J. In *Photon Correlation and Light Beating Spectroscopy*; Cummins, H. Z., Pike, E. R., Eds.; Plenum: New York, 1974; p 151.
(43) Koppel, D. E. *J. Chem. Phys.* **1972**, *57*, 4814.
(44) Provencher, S. W. *Makromol. Chem.* **1979**, *180*, 201.
(45) Bantle, S.; Schmidt, M.; Burchard, W. *Macromolecules* **1982**, *15*, 1604.
(46) Huber, K.; Burchard, W.; Akcasu, A. Z. *Macromolecules* **1985**, *18*, 2743.
(47) Adolf, D. B.; Tirrell, M. *J. Rheol.* **1986**, *30*, 539.
(48) The coefficient of the logarithmic term ($=^9/_8$) in the Brenner–Gajdos theory follows directly from the result for motion of a sphere near a plane wall and, hence, for small λ_S, should be independent of the pore space geometry. Although the coefficients of the terms linear in λ_S and other higher order terms depend on the pore geometry, the actual coefficients (at least of the linear term, the most important for consideration at low λ_S) should not differ greatly, because of pore wall curvature. For example, the result analogous to the center-line theory, for radial motion of a sphere in the center of a spherical external boundary,[1] gives a coefficient of 2.25. Although the partitioning coefficient $(1 - \lambda_S)^2 = (1 - \kappa\lambda_H)^2$ which enters the

Brenner–Gajdos theory is not correct for flexible polymers, it should be a reasonable approximation for small λ_H.
(49) Baumgärtner, A.; Muthukumar, M. *J. Chem. Phys.* **1987**, *87*, 3082.
(50) Kremer, K.; Binder, K. *J. Chem. Phys.* **1984**, *81*, 6381.
(51) van Brakel, J.; Heertjes, P. M. *Int. J. Heat Mass Transfer* **1974**, *17*, 1093.
(52) Pismen, L. M. *Chem. Eng. Sci.* **1974**, *29*, 1227.
(53) Katz, A. J.; Thompson, A. H. *Phys. Rev. Lett.* **1985**, *54*, 1325.
(54) Bohrer, M. P. *Ind. Eng. Chem. Fundam.* **1983**, *22*, 72.

Soluble Ethylmercapto-Substituted Polythiophenes

Jose P. Ruiz, K. Nayak, Dennis S. Marynick,* and John R. Reynolds*

Department of Chemistry, The University of Texas at Arlington, Arlington, Texas 76019.
Received May 17, 1988; Revised Manuscript Received September 9, 1988

ABSTRACT: Polymers of 3-(ethylmercapto)- and 3,4-bis(ethylmercapto)thiophenes have been synthesized and characterized. These polymers are soluble in common organic solvents such as methylene chloride, chloroform, and THF. Structural characterization using FT-IR and NMR spectroscopy show that these polymers have a well-defined β-(ethylmercapto)-substituted 2,5-(thienylene) polymeric structure. Visible–near-IR absorption spectra of electrochemically doped cast films and chemically doped solutions of the polymers show that they can be oxidized to form bipolaronic species. GPC studies show a number average molecular weight of about 2500 ($M_w/M_n \sim 5$) for both polymers. Maximum electrical conductivities of 10^{-3} Ω^{-1} cm^{-1} for the 3-(ethylmercapto)- and 10^{-7} for the 3,4-bis(ethylmercapto)-substituted polymers have been obtained in the oxidized state. Experimental results are correlated with theoretical calculations by using the PRDDO and extended Hückel methods, which demonstrate radical-cation reactivites for the thiophene monomers, along with minimum energy conformations and band structures in these substituted polymers.

Introduction

In the last decade, there has been considerable interest in the study of electronically conducting polymers. These efforts can be attributed to the large number of potential applications for such materials and scientific curiosity in the ability of organic materials to conduct charge.[1] The most promising of these materials should demonstrate good solution or melt processability, environmental stability, good mechanical properties, and controllable conductivities.

To improve the physical and electronic properties of these polymers, much work has been done in altering the synthetic conditions and molecular architecture of aromatic polyheterocycles, including polythiophenes, polypyrroles, and polyfurans.[2] It has been found that by placing β-position substituents on polythiophenes, highly conducting (ca. 10^{+1} Ω^{-1} cm^{-1}), yet soluble polymers are formed. Initially, Elsenbaumer et al.[3] reported a series of 3-alkylthiophene polymers that were soluble in common organic solvents. Their solubility increased with the size of the substituents, while having little effect on the maximum conductivity. Similar results have also been reported by Sato et al.[4] Due to their solubility in typical organic solvents, solution spectroscopic studies have been carried out by Heeger et al.[5,6] Recently, conducting polymers prepared from β-substituted thiophenes were reported by Bryce et al.[7] that not only are soluble but in some cases had elevated conductivities (ca. 10^{+3} Ω^{-1} cm^{-1}) relative to the unsubstituted parent, polythiophene. To date there have been two brief reports on the preparation of mercapto-substituted polythiophenes.[3,8] In both cases relatively low maximum conductivities, on the order of 10^{-1} Ω^{-1} cm^{-1}, were reported.

The ability to process these polymers using common solution processing techniques opens up a broad area of research in conductive polymers. Here we report on the synthesis and characterization of poly[3-(ethylmercapto)thiophene] (PEMT) and poly[3,4-bis(ethylmercapto)thiophene] (PBEMT), both of which are soluble in common organic solvents and semiconducting (up to 10^{-3} Ω^{-1} cm^{-1}) in the oxidized state. We correlate our structural and electronic results to results from theoretical calculations, demonstrating the ability of theory to assist in directing experimentation.

Experimental Section

Preparation of Monomers and Polymers. 3-(Ethylmercapto)thiophene (EMT) and 3,4-bis(ethylmercapto)thiophene (BEMT) were prepared from their corresponding bromo-substituted thiophenes according to the method of Yabukov et al.[9] Both materials were purified by fractional distillation in vacuo.

Different α-halogenation procedures were used for the monomers. EMT was brominated by using a published procedure for typical brominations.[10] Pure 2,5-dibromo-3-(ethylmercapto)-thiophene was obtained after fractional distillation in vacuo. BEMT was iodinated employing the method of Barker et al.[11] to give 2,5-diiodo-3,4-bis(ethylmercapto)thiophene. Purification was carried out by reprecipitation from methylene chloride into methanol.

Solution polymerization of these 2,5-dihalogeno-substituted monomers was done via a nickel-catalyzed Grignard coupling similar to the procedures used by Kobayashi et al.[12] and Elsenbaumer et al.[3] As reported previously, 2-methyltetrahydrofuran was used as the Grignard formation solvent and nickel(II) bis(diphenylphosphino)propane dibromide [Ni(DPPP)Br$_2$] as the coupling catalyst. The polymerization was carried out under nitrogen at 130 °C for at least 70 h. The polymers were purified by reprecipitation into methanol from methylene chloride and dried under vacuum. Brick red and ochre colored powders were obtained for EMT and BEMT polymers, respectively.

Structural Identification of Monomers and Polymers. Infrared spectra were obtained by using a Digilab FTS-40 FT-IR spectrophotometer utilizing transmittance between NaCl plates for liquids and the diffuse reflectance technique (DRIFT) for solids. The DRIFT method was used instead of pressed KBr pellets due to the highly opaque nature of the polymer samples.

^{1}H NMR spectra were done on a Varian EM-360 spectrometer for all monomeric materials and a Nicolet 200 FT-NMR for polymers in deuteriated chloroform. ^{13}C NMR for all materials were obtained on the Nicolet 200 instrument.

Elemental analyses were done by Texas Analytical Laboratories (Tallahassee, FL).

Theoretical Calculations. Molecular orbital calculations were performed in order to assess the spin densities of the monomeric

0024-9297/89/2222-1231$01.50/0